Supplementary data:

Supplementary Materials and Methods

Gel filtration chromatography

Soluble protein extracts (Klp5-myc Klp6-HA, Klp5-myc *Δklp6* and *Δklp5* Klp6-HA) were prepared in buffer A (50 mM Tris-HCl pH 7.5, 10% glycerol, 0.1 mM EDTA, 100 mM NaCl, 1 mM mercaptoethanol, 5 mM ATP plus a cocktail of inhibitors, Sigma). Gel filtration chromatography was performed on a Superose-6 column by FPLC (GE Healthcare UK Ltd. Buckinghamshire, UK). The column was equilibrated with 2 column volumes of buffer A. To determine molecular weight, a parallel column was run with standards consisting of dextran (2,000 kDa), thyroglobulin (669 kDa) and a-amylase (232 kDa). 15 ml of each fraction (50 ml in total) was separated by SDS-PAGE on 10% gels and fractionated proteins were detected with individual antibodies.

Supplementary References

Daga, R.R., Yonetani, A., and Chang, F. (2006). Asymmetric microtubule pushing forces in nuclear centering. Curr. Biol. *16*, 1544-1550.

Tran, P.T., Marsh, L., Doye, V., Inoue, S., and Chang, F. (2001). A mechanism for nuclear positioning in fission yeast based on microtubule pushing. J. Cell Biol. *153*, 397-412.

Radcliffe, P.A., Hirata, D., Vardy, L., and Toda, T. (1999). Functional dissection and hierarchy of tubulin-folding cofactor homologues in fission yeast. Mol. Biol. Cell *10*, 2987-3001.

Yamashita, A., Sato, M., Fujita, A., Yamamoto, M., and Toda, T. (2005). The roles of fission yeast Ase1 in mitotic cell division, meiotic nuclear oscillation and cytokinesis checkpoint signaling. Mol. Biol. Cell *16*, 1378-1395.

Supplementary Table S1: Strain List

Strains	Genotypes	Derivations
AR065	*h⁻ klp5⁺-GFP-kan pREP1(mRFP-atb2⁺)*	This study
AR066	*h⁻ klp5⁺-GFP-kan klp6::ura4⁺ pREP1(mRFP-atb2⁺)*	This study
AR067	*h⁺ ade6-216 klp5::ura4⁺ klp6⁺-GFP-kan pREP1(mRFP-atb2⁺)*	This study
AR085	*h⁻ klp6⁺-GFP-kan pREP1(mRFP-atb2⁺)*	This study
AR356	*h⁻ klp5⁺-13myc-kan klp6⁺-3HA-hph*	This study
AR399	*h⁻ klp6N(1-410)::ura4⁺::klp5N(1-404)-GFP-nat*	This study
AR445	*h⁺ his2 klp5N(1-404)::ura4⁺::klp6(1-403)-GFP-nat*	This study
AR600	*h⁻ klp5::nat klp6⁺-3HA-hph*	This study
AR602	*h⁻ klp5⁺-13myc-kan klp6::ura4⁺*	This study

All strains listed in this table contain *leu1-32 ura4-D18*.

Legends for Supplementary Figures

Figure S1: Nuclear accumulation of Klp5 and Klp6 in the presence or absence of LMB

Strains containing either Klp5-GFP or Klp6-GFP were transformed with the plasmid pREP1-mRFP-atb2^{+} (Yamashita *et al*., 2005) to visualise microtubules and observed using fluorescence microscopy under repressed conditions. Still images of live cells are shown. (A-D) Localisation of Klp5-GFP (A, B) or Klp6-GFP (C, D) in wilt type (A, C), *Δklp6* cells (B) or *Δklp5* cells (D). Representative images before (first and second panels) or after LMB addition (90 min, third and fourth panels) are shown during mitosis (first and third panels) or interphase cells (second and fourth panels). Cytoplasmic astral microtubules and dim nuclei are marked with arrowheads and arrows respectively. After LMB addition, both Klp5 and Klp6 accumulate in the nucleoplasm (diamonds) or localise to nuclear spindles in the absence of their counterpart (asterisks). Scale bars, 10 μm. (E) Line profiles of fluorescence intensity showing extent of nuclear accumulation during interphase after addition of LMB (60 min) in individual strains shown in (A-D). n=5 for each strain.

Figure S2: Klp5 and Klp6 forms a large complex in the cell

(A) Gel filtration chromatography. Soluble cell extracts were prepared from strains containing Klp5-myc Klp6-HA (wild type), Klp5-myc *Δklp6* (*klp6* deletions) or *Δklp5* Klp6-HA (*klp5* deletions) and loaded onto Superose 6 columns. Each fraction together with total extracts (20 μg, lane 1) was run on SDS-PAGE and immunoblotting was

performed with anti-Myc and anti-HA antibodies. In all cases, Klp5 and Klp6 existed in large fractions (~2000 kDa). As a control to show a successful fractionation of extracts, anti-a-tubulin antibody was used to detect fractionation patterns of α-tubulin (Radcliffe *et al.*, 1999). As expected, α-tubulin was fractionated at two positions, one at ~2000 kDa and the other at ~232 kDa. Positions of the void volume and various size markers (corresponding to 2,000 kDa, 669 kDa and 232 kDa) are shown with an arrowhead and horizontal lines respectively.

Figure S3: Quantification of nuclear accumulation of chimeric Klp5/6-GFP molecules upon LMB treatment

Line profiles of fluorescence intensity showing nuclear accumulation of GFP-tagged chimera constructs (shown as cartoons) in Klp5 and Klp6 during interphase upon LMB treatment (60 min after addition). See Figure 1E for Klp5-GFP or Klp6-GFP controls cells. n=5.

Note: To understand why the Klp6N/5C-GFP chimera fails to localise to the nucleus, we quantified the extent of nuclear accumulation of GFP signal after LMB addition as in Supplementary Figure S1E. It was evident that Klp6N/5C-GFP does not accumulate in the interphase nucleus at all in response to LMB (B). In contrast, the Klp5N/6C-GFP chimera was capable of localising to the nucleus under the same conditions (A) although there was some degree of heterogeneity between cells. It was also noticeable in the same strain that the regions of high fluorescence intensity were not always centred within the cell. In wild type cells, the nucleus is positioned at the geometric centre by microtubule-mediated pushing (Tran *et al.*, 2001; Daga *et al.*, 2006). As shown earlier (Figure 5C), microtubule dynamics seem to be perturbed in Klp5N+Klp5N cells, which would make it

likely that nuclear positioning is also affected in this strain. These experiments indicate that construction of a chimera consisting of Klp6N/5C (Klp6N+Klp6N) interferes with the NLS located in the C-terminal tail, leading to nuclear import defects, whilst the reciprocal construct Klp5N/6C (Klp5N+Klp5N) is capable of entering the nucleus, but is highly toxic and impedes cell cycle progression.

Figure S4: Microtubule growth and shrinkage rates in various *klp5/6* mutants

In order to present the rate of microtubule growth (A) and shrinkage (B) in a more quantitative manner (shown in Figure 6A and B), box-and-whisker plots are applied.

Figure S5: Interphase microtubule dynamics in various *klp5/6* mutants

The data showing the percentage of time spent (shrinkage, pause, growth at a free end or a cell tip) is presented. In our measurements, microtubules in all the strains examined continue to grow at the cell end

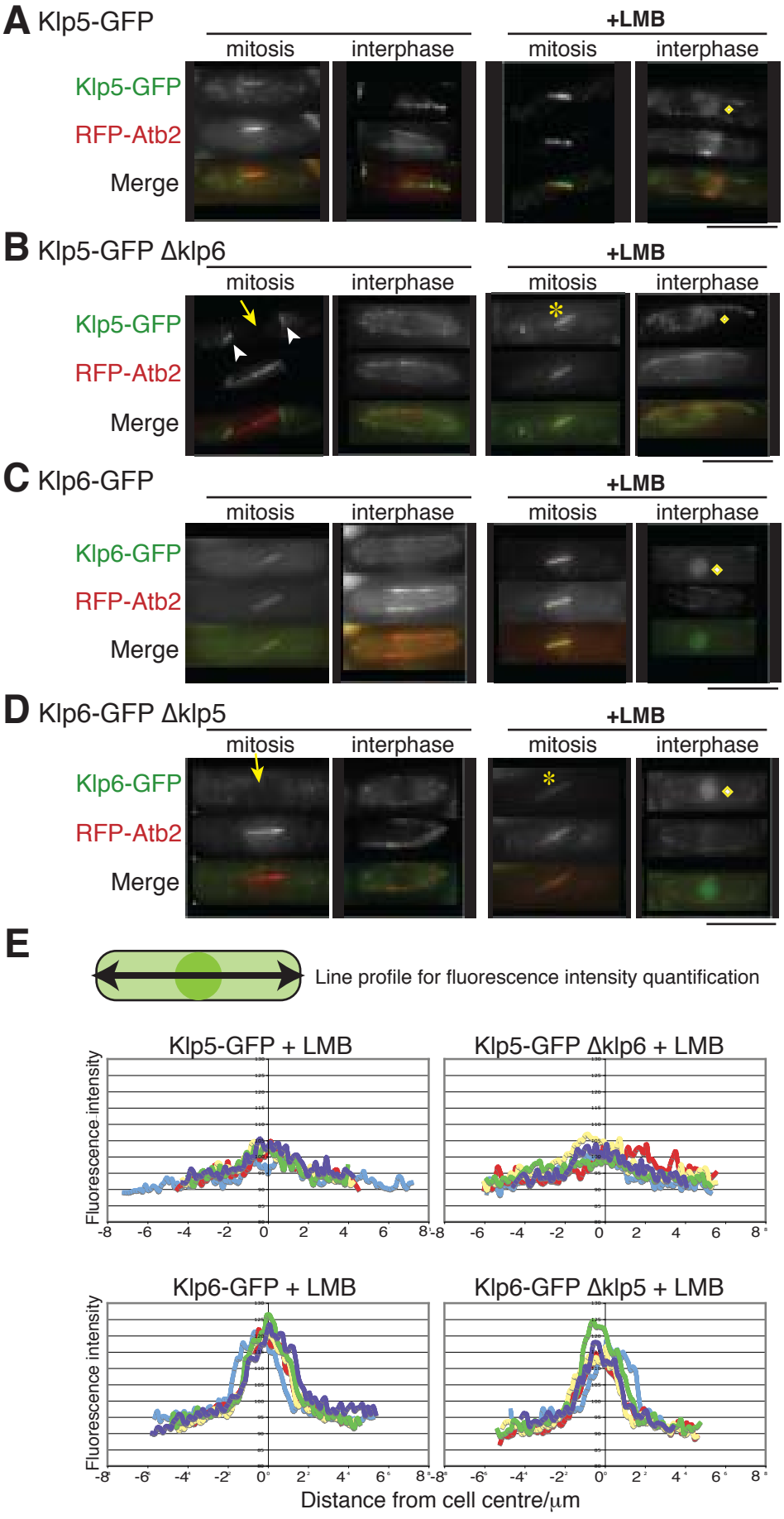

Supplementary FigureS1: Unsworth et al.

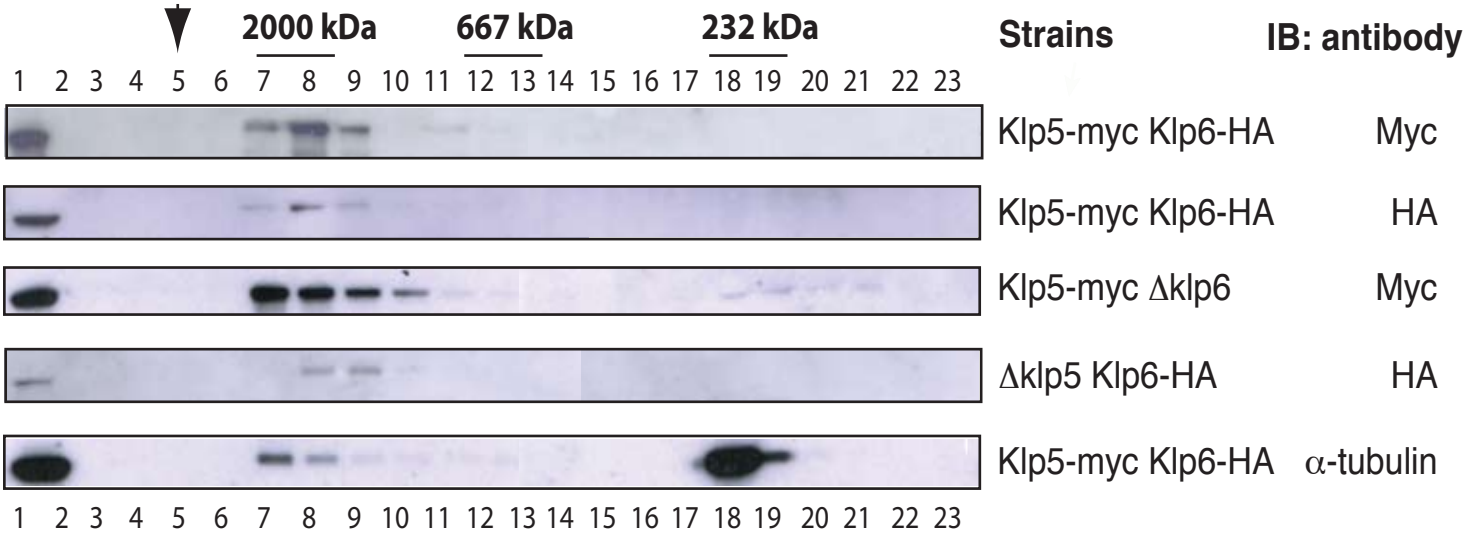

Supplementary FigureS2: Unsworth et al.

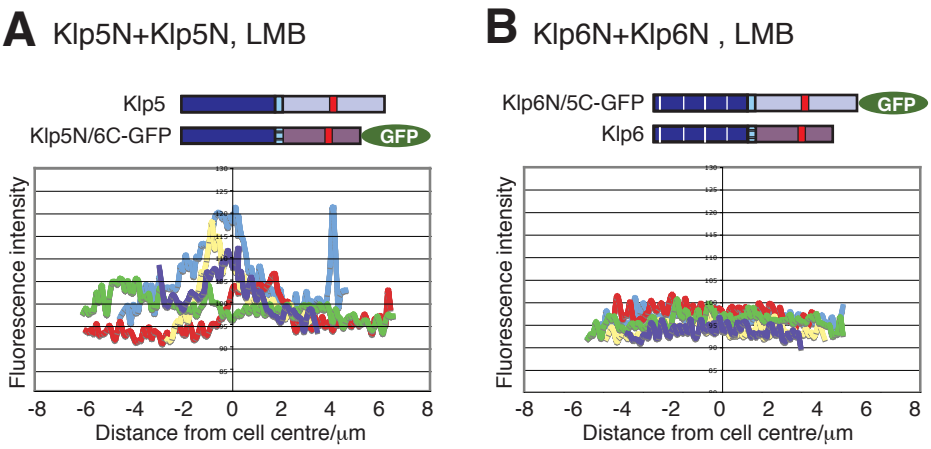

Supplementary FigureS3: Unsworth et al.

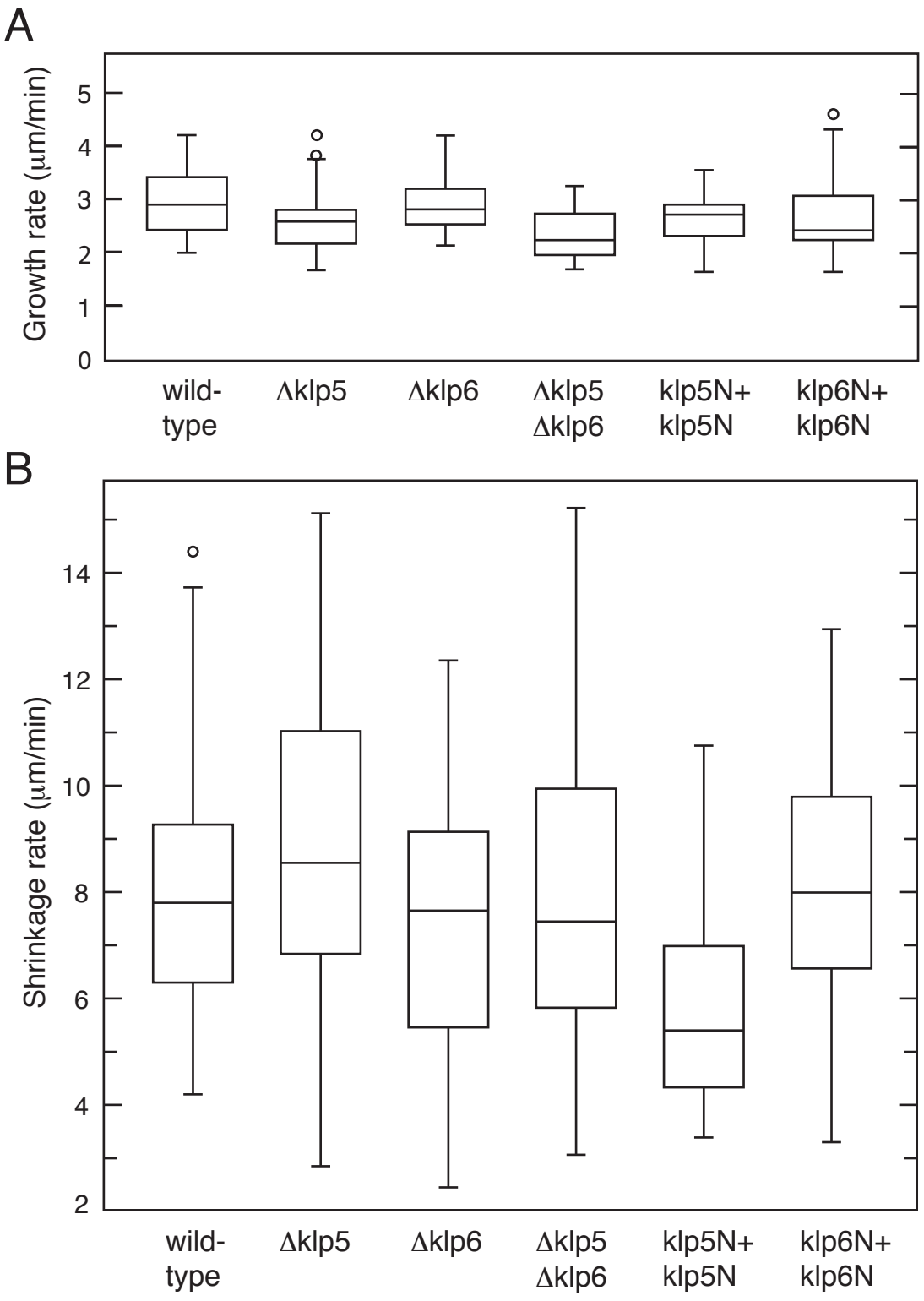

Supplementary FigureS4: Unsworth et al.

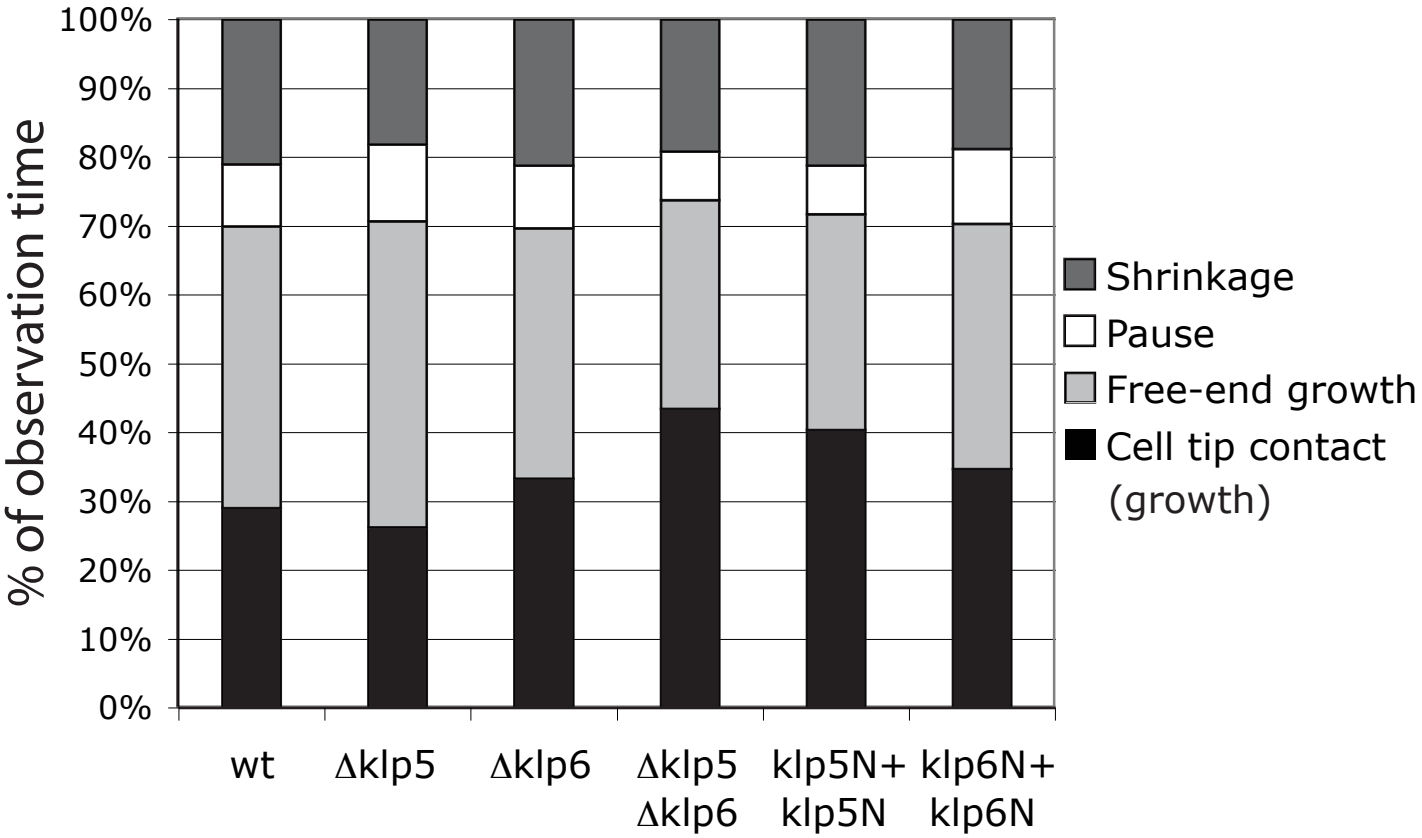

Supplementary FigureS5: Unsworth et al.